Journal of Materials Chemistry A

Accepted Manuscript

ROYAL SOCIETY OF CHEMISTRY

www.rsc.org/materialsA

Journal of Material Chemistry A

ARTICLE

Nanocolumnar 1-dimensional TiO_2 photoanodes deposited by PVD-OAD for perovskite solar cells fabrication

Received 00th January 20xx,
Accepted 00th January 20xx

DOI: 10.1039/x0xx00000x

www.rsc.org/

F. Javier Ramos[a], Manuel Oliva-Ramirez[b], Mohammad Khaja Nazeeruddin[c,d] Michael Grätzel[d], Agustín R. González-Elipe[b] and Shahzada Ahmad[a]*

Perovskite solar cells have attracted an increasing interest among the photovoltaic community in the last years owing to their unique properties and high efficiency. In the present work, we report the fabrication of perovskite solar cells based on highly ordered 1-dimensional porous TiO_2, which are uniform on a large area. These nanocolumnar porous TiO_2 photoanodes were deposited by physical vapor deposition in an oblique angle configuration (PVD-OAD) by varying the zenithal angle between the target and the substrate normal. Perovskite infiltration into these 1-dimensional nanocolumnar was homogeneous through the entire thickness of the porous layer as revealed by secondary ion mass spectroscopy studies. The fabricated solar cells, with optimized thickness of photoanode and with industrially accepted methods will pave the way for easy to implementation at large scale.

A Introduction

Perovskites based solar cells have attracted surge of attention in very short time frame owing to their remarkable power-conversion efficiency (PCE) which can match those of well-established and mature technologies[1–4]. The light harvesting abilities in these devices has positioned them as a strong competitor within the thin film category of solar cells with PCE approaching to 20% in laboratory[5,6]. The versatility of the perovskite deposition, by wet chemistry[1,3,5,6], vapor deposition [7] or mixed process comprising solution process for the inorganic precursor followed by a vapor assisted deposition of the organic component[8] makes it attractive for the manufacturing of a large variety of cell architectures. These deposition method have proved to be compatible with different photoanode materials like the most extended TiO_2[3,5,6,9], ZnO[10,11] or even mesoporous scaffolds made of electron non-injecting oxides like Al_2O_3[2,12] or ZrO_2[13]. The classical hole transporting materials (HTM) Spiro-OMeTAD[1–3,6], as well as others polymeric[5,14], organic[15,16] and inorganic[17] were found suitable for efficient device fabrication, though the use of HTMs is not mandatory [9]. The high open-circuit potential in these devices are due to their low thermodynamic losses. Thus, for a bandgap of 1.55 eV ($CH_3NH_3PbI_3$)[18], V_{oc} values of 1.2 V can be achieved, mainly due to the low recombination rate characteristic of these systems.[19,20]

In the past, the application of vertically-aligned nanostructures (nanocolumns, nanorods, nanowires) was found to be effective to enhance electron transport properties for different types of solar cells including silicon[21], III-V semiconductors[22], organic photovoltaics[23] and dye sensitized solar cells (DSSC)[24–26]. In addition, the idea of using these nanostructured nanocolumnar thin films is not only justified by the expected improvement of the transport properties along the nanocolumns, but also because as low-refractive index materials they can minimize the reflection of light, thereby enhancing the amount of absorbed light and can push the efficiency of solar cell. The fabrication of nanostructured columnar thin films has been intended by different techniques, including the physical deposition method at oblique angles[27,28]. In DSSCs this technique was found to be effective for increasing the amount the absorbed dyes to harvest light, to improve the transport properties and carriers lifetime, all these features leading to photogenerated current improvements with respect equivalent mesoporous nanoparticle cells[27,29]. Based on that concept, herein we have produced TiO_2 aligned nanocolumnar photoanodes by the physical vapor deposition method at oblique incidences angles (PVD-OAD) and used them for the fabrication of $CH_3NH_3PbI_3$ based solar cells. To further tune and optimize the system, the influence of different morphological parameters such as porosity, thickness and angle arrangement of the nanocolumnar layers was investigated to check their influence

[a] Abengoa Research, Abengoa, C/ Energía Solar no 1, Campus Palmas Altas, 41014, Sevilla, Spain. Email: shahzada.ahmad@abengoa.com
[b] Instituto de Ciencia de Materiales de Sevilla, (CSIC-Universidad de Sevilla), c/Americo Vespucio 49, 41092 Sevilla, Spain.
[c] Group for Molecular Engineering of Functional Materials, Institute of Chemical Sciences and Engineering, École Polytechnique Fédérale de Lausanne, CH-1015-Lausanne, Switzerland
[d] Laboratory of Photonics and Interfaces, Department of Chemistry and Chemical Engineering, École Polytechnique Fédérale de Lausanne, Station 6, CH-1015 Lausanne, Switzerland.

Electronic Supplementary Information (ESI) available: Optimization of the perovskite recipe for the NC-TiO_2 photoanodes, histograms of devices and transient photocurrent measurement of nanocolumnar perovskite solar cells. See DOI:

on photovoltaic performance magnitudes such as short circuit current (J_{SC}), open-circuit voltage (V_{OC}), fill factor (*FF*) or PCE.

It is important to remark that uniform and large area 1-directional nanocolumnar photoanodes can be easily prepared using this PVD technique, which is critical for future up scaling of the technology. To visualize the degree of infiltration of the perovskites in the pores of the film, Time of flight-secondary ion mass spectrometry (ToF-SIMS) was used to analyze the perovskite distribution along the photoanode thickness. It has been found that the adequate infiltration of the perovskite inside the nanocolumnar film is an critical condition by the fabrication of these structures and that it can be moderately tuned by varying the porosity of the film by changing the zenithal incidence angle (α) of the evaporated flux of TiO_2 onto the substrate.

In the past[30–32] nanocolumnar and nanowires TiO_2 based photoanodes (thickness 500-1500nm) was utilized for perovskite solar cells fabrication and thinner film were found to effective for device fabrication, similar to this we found that TiO_2 photoanodes (between 200-300nm) are even more efficient to collect the photons and, likely because of their particular tilted microstructure[28], showing high J_{SC} values (>16 mA cm^{-2} for 200nm and even >18 mA cm^{-2} for the 300nm thick one) in combination with very high V_{oc} 949.8mV and good fill factor (~0.64) consequence of the good transport of charge along the nanocolumns gave PCEs of 10.52%.

B Experimental

Materials. All chemicals were commercial either Sigma Aldrich or Agros and were employed without any treatment or purification. 2,2',7,7'-tetrakis(*N,N*-di-p-methoxyphenyamine)-9,9-spirobifluorene (Spiro-OMeTAD) was acquired from Merck KGaA. Poly-triarylamine (PTAA) was acquired from EM-index (Mw=17500g mol^{-1}). Methylamine iodide, CH_3NH_3I (MAI), was synthetized according the known literature[33].

Preparation of TiO_2 tilted nanocolumnar films. *NC*-TiO_2 anatase used as electron transporting porous films with a thickness from 100 to 500nm were prepared at room temperature by physical vapor deposition at oblique incidence (PVD-OAD) along a procedure reported in previous publications[27–29]. Basically, this method consists on a physical vapor deposition where the substrate surface is placed forming a glancing angle with respect to the evaporation source. A zenithal evaporation angle (α) is defined between the normal to the substrate and the flux of evaporation material as illustrated in Fig. 1a. Varying the mentioned zenithal angle, the tilting angle of the nanocolumns can be tuned, as well as the porosity and other properties of the films[28].

Device fabrication. Firstly, FTO-coated glass, TEC15 from Pilkington, was patterned by laser etching. Then, the substrates were cleaned using Hellmanex solution and rinsed[11,19] with deionized water and ethanol; subsequently they were ultrasonicated in 2-propanol and rinsed again using ethanol and acetone and finally dried with compressed air. Prior to the compact layer deposition, the samples were cleaned with an ultraviolet/O_3 treatment during 30 minutes.

A TiO_2 compact layer was deposited by spray pyrolysis at 450°C using 0.5mL of titanium diisopropoxide bis(acetyl acetonate) precursor solution (75% in 2-propanol, Sigma Aldrich) in 19.5mL of absolute ethanol using O_2 as carrier gas. After finishing the spray pyrolysis deposition, the samples were kept for another 30 minutes at 450°C to facilitate the anatase formation. Once the samples are at room temperature, they are subjected to a $TiCl_4$ treatment, immersing them in a 0.02M $TiCl_4$ solution in deionized water at 70°C for 30 minutes. This was followed by washing with deionized water, heated at 500°C for 15minutes and left to cool down slowly until room temperature.

After that, the porous electron transporting layers (TiO_2 tilted nanocolumns) were deposited according the above mentioned procedures. For the mesoporous devices, 18NR-T paste (Dyesol) was diluted in absolute ethanol (1g paste in 3.5g of ethanol) and deposited by spin coating at 5000rpm for 30s.

Later, perovskite was prepared by sequential deposition, following the currently reported article guidelines for high-performance perovskite cells[3]. Therefore, a lead iodide (PbI_2) film was deposited by spin coating (6500rpm for 30s with 5500rpm s^{-1} as acceleration) using 50μL per cell of PbI_2 solution in N,N-dimethylformamide (DMF) that was kept at 70°C under vigorous stirring. To avoid insolubility issues, the PbI_2 solution in DMF was previously dissolved at 115°C and cold down until reaching 70°C, temperature which is maintained during the whole PbI_2 deposition process. After the spin coating process, the cells were placed onto a hot plate at 70°C for 30 minutes for annealing. After cooling down the samples to room temperature, the cells were dipped in the MAI solution in 2-propanol (8-10mg mL^{-1} depending the case) for 20s, moment when the change of color from yellow to dark brown-black is observed; when prewetting technique was employed, the samples were dipped in pure 2-propanol for 5s before dipping for 30s in the MAI solution. Subsequently they were rinsed in 2-propanol and dried using the spin coater at 4000rpm for 30s, finally it was annealed again at 70°C for 30 minutes.

The hole transporting materials (HTM) was deposited after: either using Spiro-OMeTAD or PTAA. For Spiro-OMeTAD, 35μL of solution were dropped on substrates and deposited by spin coating at 4000rpm for 30s using an acceleration of 1650rpm s^{-1}; for PTAA, 2000rpm for also 30s were selected. Spiro-OMeTAD solution was made dissolving 72.3mg of Spiro-OMeTAD in 1mL of chlorobenzene; 21.9μL of tris(2-(1H-pyrazol-1-yl)-4-tert-butylpyrydine)cobalt(III) bis(trifluoromethylsulphonyl)imide (FK209) stock solution (400mg of FK209 in 1mL of acetonitrile), 17.5μL of lithium bis(trifluoromethylsulphonyl)imide (LiTFSI) stock solution (520mg of LiTFSI in 1mL of acetonitrile) and 28.8μL of 4-tert-butylpyridine (t-BP) were also added to the solution as additives. PTAA solution was prepared dissolving 30mg of PTAA in 1mL of toluene; 18.8μL of lithium LiTFSI stock solution (170mg of LiTFSI in 1mL of acetonitrile) and 9.4μL of t-BP were added as well. The device fabrication was finished with an

80nm of gold as metallic contact (cathode) deposited by thermal evaporation under a vacuum ($1{\cdot}10^{-6}$ and $1{\cdot}10^{-5}$torr). PbI_2, MAI, Spiro-OMeTAD and PTAA solutions were prepared inside an argon glove box with controlled moisture and oxygen conditions (H_2O level :< 1ppm and O_2 level: <10ppm). PbI_2 spin coating, MAI dipping and HTM spin coating depositions were developed inside a dry box.

Characterization. For *J-V* curves, a 450W Xe lamp (Oriel) with a Schott K113 Tempax sunlight filter (Praezisions Glas & Optik GmbH) was employed as a light source. A digital source meter (Keithly Model 2400) was used to apply the voltage to the cell while current was recorded. Sun intensity was measured just before each single device with the help of a Si reference cell.

For IPCE measurements, a 300W Xe lamp (ILC Technology) was connected to a Gemini-180 double monochromator (Jobin Yvon Ltd.) to get an appropriated light beam. A constant white light bias (5%-10% of the received light) was found recommendable to measure perovskite cells, so an array of white LEDS were used for that purpose. A Model SR830 DSP Lock-in Amplifier (Standford Research Systems) was utilized to record the performance. Both for *J-V* and IPCE measurements the active area was fixed to 0.285cm^2 using a mask unless other indications were specified at a scan rate of 0.1V/sec. The scan rate and the active area used for measuring the devices were optimized as such to calculate the real value for efficiencies without having hysteresis effect. To measure the absorbance spectra of the cells, a (Hewlett Packard 8453) spectrophotometer was used. The scanning electron microscopy images were imaged by a field-emission scanning electron microscope (FE-SEM) using a Hitachi S5200 field emission microscope operated at 5.0 keV.

C Results and discussion

A schematic configuration of the Physical Vapor Deposition at oblique angles (PVD-OAD) is shown in Fig. 1a where it is apparent that by controlling the position of the samples along the x-axis it is possible to select a given zenithal deposition angle (α). Basic characteristic of the PVD-OAD method is that both the tilting angle of the nanocolumns and the porosity of the film can be tuned by adequately regulating the deposition angle:α[27–29]. In general, the porosity and the tilting angle of nanocolumns increase with the deposition angle, having been previously reported tilting angles (β) of 34° and 47° and porosities of 49% and 67% (v/v) were obtained for TiO_2 thin films deposited at zenithal angles (α) of 70° and 85°, respectively[28]. Fig. 1b shows a scheme of a cell device incorporating a TiO_2 nanocolumnar thin film structure as photoanode. To confirm the shape of the nanocolumnar TiO_2 layer, Scanning Electron Microscopy (SEM) studies were carried out. Fig. 2a and Fig. 2b show cross section SEM micrographs of the nanocolumnar films deposited on silicon wafer for the two zenithal evaporation angles (α=70° and 85°) employed in the present work. These micrographs shows that α=70° (Fig. 2a) renders less tilted nanocolumns (tilting angle β=34°) than α=85° (β=47°) (Fig. 2b) and confirm that the 85° film is less compact and presents a higher porosity than the 70° film in agreement with previous results.[27,28] In Fig. 2c , a top view SEM from a nanocolumnar PVD-OAD TiO_2 film deposited on silicon confirms that the nanocolumns are extremely well ordered and homogeneously packaged, features that contrast with the microstructures of TiO_2 thin films obtained by chemical routes generally characterized for an uneven distribution of their building blocks. When the perovskite film is deposited on the surface of this TiO_2 (Fig. 2d)

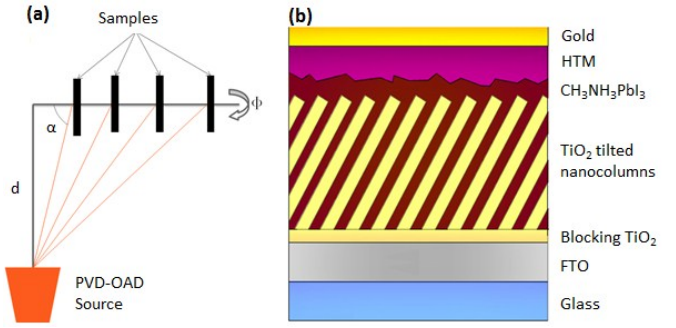

Figure 1. a) Schematic configuration for the physical vapor deposition at glancing incidence (PVD-OAD) technique employed for the TiO_2 tilted nanocolumns[27], b) Schematic representation of the perovskite-sensitized solar cells using the tilted nanocolumns as photoanode.

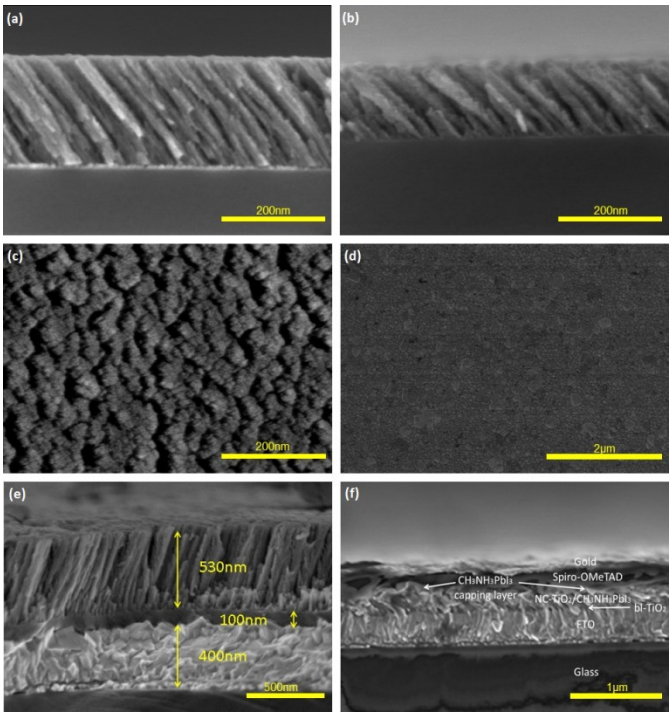

Figure 2. Cross sectional scanning electron microscopy (SEM) images of, a) of the TiO_2 tilted nanocolumnar TiO_2 photoanode deposited by PVD-OAD with 70° as glancing angle (α), b) cross section of the NC-TiO_2 film deposited with 85° as α, c) top view image of the NC-TiO_2 film. d) top view of the perovskite formed over the NC-TiO_2 film, e) cross sectional SEM image of NC-TiO_2 film with perovskite infiltrated. f) cross sectional SEM image of full device. Note the Fig.2a is more focused and zoomed.

it forms a very conformal capping layer terminated in a flat surface, a condition required for highly efficient perovskite solar cells. To illustrate the topology of the system when it is prepared on FTO glass containing the compact TiO_2 layer, the

SEM micrograph in Fig. 2e shows a cross section after deposition of the perovskite. From bottom to top of this image, layers due to FTO (400 nm), compact TiO_2 (ca. 100 nm), nanocolumnar TiO_2 deposited by PVD-OAD (ca. 530 nm, thicker than the optimum value for better visualization) and perovskite (ca. 100 nm) are clearly distinguished. A cross section of the full cell device with a 200 nm thick TiO_2 layer and including the hole collector layer and the gold upper electrode is shown in Fig. 2f. In this figure there is some hints that the TiO_2 nanocolumnar film deposited at 85o is infiltrated by the perovskite (i.e., it consists of a NC-TiO_2/$CH_3NH_3PbI_3$ hybrid layer). Over this photoanode, a capping $CH_3NH_3PbI_3$ layer and a ~150nm thick Spiro-OMeTAD overlayer can be also observed. Overall, these two images show that the subsequent deposition of the different layers stacked in the cell according to the scheme in Fig. 1b proceeds homogeneously in a layer by layer fashion without patches or large inhomogeneities.

To prove the homogeneous infiltration of the perovskite within the pores of the TiO_2 nanocolumnar films, ToF-SIMS measurements were carried out with the FTO/NC-TiO_2/$CH_3NH_3PbI_3$ structure depicted in Fig. 3. Fig. 3 shows the elemental depth profiles obtained for this structure where a rather thick NC-TiO_2 photoanode (530nm) has been included to prove the excellent infiltration properties of the perovskite material even for a less advantageous case. This figure shows the evolution of the peaks intensity as a function of the etching time for selected ion masses corresponding to Ti^+, SiO^+, Sn^+, PbO^+ and Pb^+ species. An attribution of depth zones according to the scheme in Fig. 1b is included in the depth profiles figure. The lead species (PbO^+ and Pb^+) can be taken as a probe of the distribution of the perovskite within the NC-TiO_2 layer. Other species such as I^+, ionized methyl and ammonia groups and other fragments of the perovskite structure were also detected during this investigation and presented profiles that run in parallel to those of Pb^+ and PbO^+. The most outstanding feature from this analysis is that the Ti^+ signal in the zone corresponding to the porous TiO_2 runs parallel to the signals attributed to the perovskite, a feature demonstrating that $CH_3NH_3PbI_3$ has been completely infiltrated within the NC-TiO_2 film and it is well distributed through its pore structure. Also, a closer look to the plots in Fig. 3 provides some additional information about the different layers existing in the perovskite solar cell. For example, looking to the initial stages of the ion etching process it is apparent that the Pb^+ and Ti^+ lines have, respectively, slightly higher and lower intensities than in the central plateau of the profile. This agrees with the cross sections in Fig. 2e and Fig. 2f and, particularly, Fig. 2d (SEM images), showing that a thin perovskite layer is covering the NC-TiO_2 film in the form of a capping layer. Similarly, the Pb^+ line decreases previous to that of the Ti^+ signal, confirming the existence of a 100 nm compact TiO_2 layer at the bottom of the structure (Fig. 2e and Fig. 2f). On the other hand, the line attributed to Sn^+ must proceed from the FTO substrate since it sharply increases in intensity when etching this zone of the structure. Moreover, the stepped shape of the Sn^+ profile with some minute intensity within the "100 nm TiO_2 zone" suggests some minor diffusion (note the logarithmic scale of the plot) of tin within this TiO_2 layer during the different annealing treatments of the system.

To fabricate efficient devices, some preliminary studies with the same TiO_2 nanocolumnar film were developed to optimize the perovskite deposition methodology. The selected thickness to carry out these previous studies was 300nm, since this value is common in the works using mesoporous TiO_2 based systems[3]. Meanwhile, the deposition angle was chosen at 70°

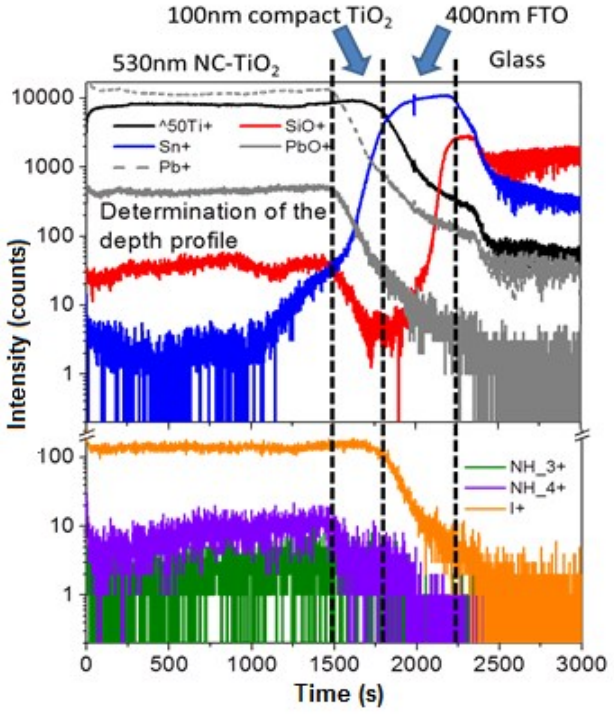

Figure 3. Time of Flight Secondary Ion Mass Spectrometry (ToF-SIMS) profiles for Ti^+, SiO^+, Sn^+,PbO^+, Pb^+, I^+ and $NH_3^+(NH_4^+)$ species proving the homogenous distribution of the perovskite through the porous structure of the 530nm thick NC-TiO_2/$CH_3NH_3PbI_3$ film.

similar TiO_2 PVD-OAD films were previously tested in liquid DSSCs[27]. The obtained results are summarized in the Table S2 and the *J-V* curves shown in Fig. S1. It was found that a gain in V_{OC} and a drop in J_{SC} are observed when methyl ammonium iodide (MAI) concentration is increased until 10mg mL^{-1}. The best CH_3NH_3I concentration was then established at a compromise value of 8mg mL^{-1}. On the other hand, regarding the lead iodide, the J_{SC} remained relatively high and stable around 18mA cm^{-2} up to concentrations of 1.45 M, when it starts to decrease. An analogous evolution was found for the fill factor that remained relatively stable at around 0.6 with the exception of a decrease observed for the most concentrated solutions. Meanwhile a maximum value of V_{OC} was found for 1.25 M solutions, conditions that also yield an optimum value of the PCE of the device. Therefore 1.25 M for PbI_2 and 8mg mL^{-1} for MAI solutions were taken as the best conditions for the deposition of the perovskite over the 300nm NC-TiO_2 photoanodes, obtaining 10.22% of PCE at full sun and a slightly higher efficiency (10.39%) for 10% of sun light. Increasing the loading of PbI_2 (chromophore) to 1.25M increase the light harvesting capability of the system, however at much higher

loading it may slow down the conversion process of perovskites.

Next, a study of the photoanode architectures was carried out to check the influence of thicknesses and evaporation angles in the performance of the devices. A summary of the obtained results is shown in Table 1 and Fig. 4. Minute differences in PCE were observed when comparing the 200 and 300nm thick photoanodes or as a function of the evaporation angle employed. The best cell was obtained with a 200nm thick NC-TiO_2 layer deposited at 85° angle, which showed a PCE of 10.53% (J_{SC}=16.68mA cm^{-2}, V_{OC}=949.8mV and *FF*=0.639).

In contrast to these optimum conditions, 100 and 500nm thick photoanodes did not render in efficient solar cells. In the former case, little J_{SC} values were determined, very likely because of a very poor conversion of incident photons into electrons (IPCE) (Fig. 5a & 5b). This suggests that not enough perovskite was deposited over and infiltrated inside these films. Moreover, for the 100nm film thickness, the 70° films were surprisingly better than the 85° ones, in apparent contradiction with the higher porosity of the latter (i.e., 67% pore volume versus 49%, respectively[27,28]). In principle, when the NC-TiO_2 film gets thicker, it is expected that more perovskite becomes infiltrated within the films, leading to a higher efficiency in photon collection and conversion into electrons, as it is shown by the IPCE curves in Fig. 5b.

Table 1. Performance of the perovskite sensitized solar cells fabricated employing TiO_2 tilted nanocolumns as photoanodes. Different thicknesses, evaporation angles (α) and two different hole transporting materials were employed.

Thickness[a] (nm)	Evaporation angle, α[b] (o)	[PbI_2] (M)	MAI concentration (mg mL^{-1})	HTM	Sun Intensity[c] (%)	J_{SC} (mA cm^{-2})	V_{OC} (mV)	*Fill Factor*	*PCE* (%)	R_s (Ω cm^2)
100	70	1.25	8	Spiro-OMeTAD	95.5	10.57	867.3	0.632	6.06	15.38
100	85	1.25	8	Spiro-OMeTAD	95.7	6.04	857.4	0.600	3.24	43.02
200	70	1.25	8	Spiro-OMeTAD	96.0	14.39	972.9	0.637	9.29	12.04
200	85	1.25	8	Spiro-OMeTAD	96.1	16.68	949.8	0.639	10.53	11.71
300	70	1.25	8	Spiro-OMeTAD	99.6	18.25	949.0	0.588	10.22	12.13
300	85	1.25	8	Spiro-OMeTAD	95.6	18.02	849.7	0.609	9.75	10.05
500	70	1	10	Spiro-OMeTAD	96	15.67	800.2	0.523	6.82	17.13
200	70	1.25	8	PTAA	95.7	7.29	825.3	0.576	3.62	25.38

[a]Thickness of the PVD-OAD TiO_2 tilted nanocolumns based photoanode. [b] For an evaporation angle α= 70° a real tilting angle β = 34° is expected, while when α= 85° the columns were more tilted (β = 47°). [c] Sun intensity was measured before measurement and calibrated with the help of a Si solar cell.

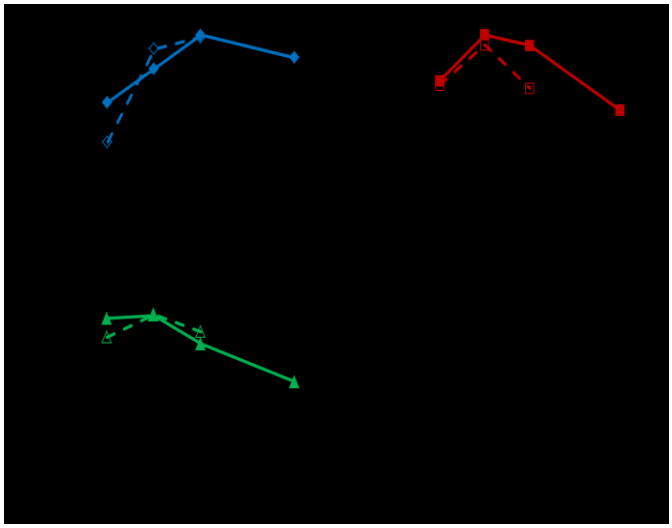

Figure 4. a) Short-circuit current (J_{SC}), b) open-circuit voltage (V_{OC}), c) fill factor and d) power conversion efficiency shown for the perovskite sensitized solar cells as a function of thickness and angle of the photoanodes deposition. Solid rhombus, squares, triangles and circles linked with solid lines were prepared with 70° as evaporation glancing angle (α). Hollow rhombus, squares, triangles and circles linked with dashed lines were prepared with 85° as evaporation glancing angle (α).

Consequently, a tradeoff maximum in the photogenerated current was found with the 300nm thick photoanodes, that presented short circuit current values similar with the maximum ones presented in literature[34,35]. When films become thicker than 300nm, J_{SC} starts to decrease again. This phenomenon has been also reported[31,32] (Table S1) and identified by a decrease in J_{SC} always that the 1-dimensional photoanode becomes thick. For the 300nm NC-TiO_2 films, no differences with the variation of the deposition angle α were observed, while for the 200nm thick films, J_{SC} did improve for the highly porous films prepared at α=85°. Concerning V_{OC}, a maximum value was also observed at 200nm, then decreasing for thicker films (Table 1, Fig. 4 and Fig. 5a). A drop in V_{OC} with photoanode thickness is in accordance with previous results in literature[31,32,34] and can be easily explained by considering that for too long 1-dimensional fibers (nanowires, nanorods or nanocolumns) recombination phenomena at the larger interface photoanode-absorber can significantly augment as well. Another interesting observation is that the *FF* decreases with the thickness of the photoanode, a feature that can be related with the increment of series resistance related with longer wires and recombination because longer columns have more surface for recombination at the interface TiO_2-perovskite and issues. This general tendency agrees with our values (Table 1, Fig. 4 and Fig. 5) with the exception of the thinnest TiO_2 layers (100nm) for which the low efficiency hampers the achievement of acceptable fill factors. Transient photocurrent experiments were carried out (Fig. S2) and it shows relatively slow response for thicker NC-TiO_2 (500 nm), while in the case of 200nm (85°) and 300nm (70°), linear response was observed, which is in well agreement with the results.

To summarize, PCE in the NC-TiO_2 based devices is directly related to J_{SC}, V_{OC} and *FF*, so that the overall efficiency of the devices is a tradeoff between these parameters. 300nm thick NC-TiO_2 photoanodes were the best in terms of current but 200nm thick ones showed a significantly better voltage performance and a higher FF and, as a result, gave the best PCE of 10.53%. The 200nm NC-TiO_2 photoanode prepared at α=85° resulted better in terms of PCE (10.53% when α=85° for only 9.29% for α=70°) due to the differences in J_{SC}. For the 300nm thick films prepared at the two deposition angles, the differences in the photovoltaic parameters were really small leading to similar PCE (9.75% when α=85°; 10.22% for α=70°). It is important to note that very homogeneous porous structures have been fabricated with the implementation of the PVD-OAD technique, obtaining efficient cells with the thinnest films reported for perovskite solar cells over nanocolumnar films[31,34,35].

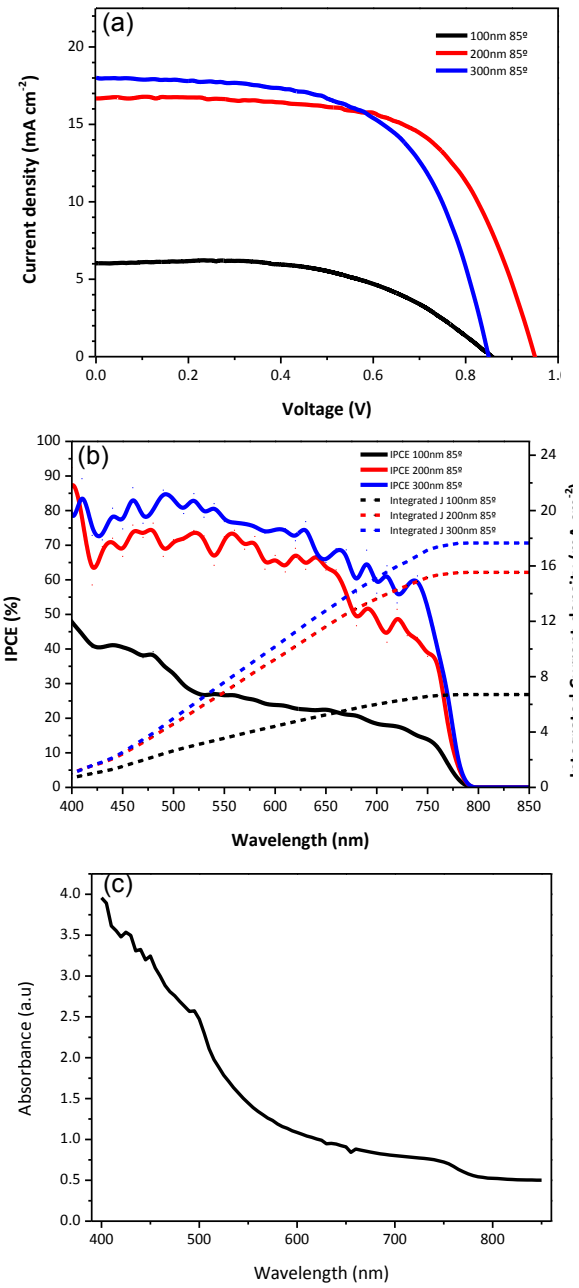

Figure 5. a) *J-V* curves for the devices prepared with nanocolumnar TiO_2 as photoanode under 1 sun for varying thickness, deposited as evaporating angle of 85° using Spiro-OMeTAD as HTM, b) the corresponding IPCE spectra and integrated photocurrent, with 5% white light bias, c) absorbance spectra for a typical cell employing 200nm TiO_2 with 85° as glancing angle as photoanode.

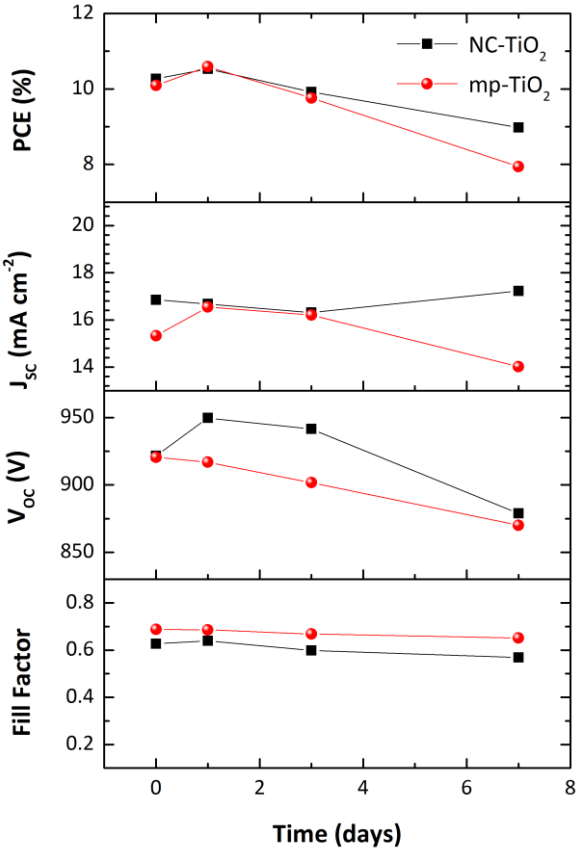

Figure 6. Evolution of the photovoltaic parameters (*PCE*, J_{SC}, V_{OC} and *FF*) for NC-TiO_2 photoanodes and standard mp-TiO_2 ones at 1 sun.

The NC-TiO_2 films prepared were also tested with a, poly(triarylamine) (PTAA) hole transporting material. The fabricated devices gave low PV performance and PCE of 3.62% (J_{SC}=7.291mA cm^{-2}, V_{OC}=825.3mV and *FF*=0.576) was measured. PTAA is a polymer with a higher molecular weight than Spiro-OMeTAD (17500 Da w.r.t only 1225.45 Da. In the case of PTAA a bilayer contact between perovskite and HTM was expected compared to the infiltrated Spiro-OMeTAD. We believe that the lower voltages and fill factors obtained here are due to in efficient charge collection through the nanocolumns indicating optimization of perovskite infiltration is required.

The absorbance spectra (Fig. 5c) for the cell devices prior to the deposition of gold show very high absorbance for the 200 nm NC-TiO_2 thick films. Fig. 6 represents, the PV parameters plotted as a function of time to evaluate the stability of the fabricated perovskite solar cells using the nanocolumnar photoanodes prepared by PVD-OAD. The devices were used as

such and were not encapsulated. The time dependent performance was then compared with a standard mesoporous (mp-TiO_2) based photoanode cell of comparable PV performance. For this experiment all solar cells were kept under dark conditions and dry air (<2% R.H.) until performing the measurement. In general, comparable trends were observed for the efficiency of both photoanode structures (NC-TiO_2 and mp-TiO_2), with the best values obtained after one day. In all like hood due to better infiltration of active materials inside the structure. However, in the case of NC-TiO_2 devices, an improvement of V_{OC} was observed after this period of time, while for the mp-TiO_2 cell this enhancement was due to a shift in J_{SC}. Regarding J_{SC}, stable values were exposed for NC-TiO_2, while short-circuit current was increased after one day and then decreases with time for mp-TiO_2 sample. *FF* was found to have negligible effect in both cases and improved efficiencies with time were obtained for NC-TiO_2 photoanodes. Thus relatively stable solar cells were obtained with the presented photoanode prepared by PVD-OAD technique due to its 1-directional orientation and less exposure of the perovskite. The calculated drop in efficiency after a week was only 14.7% (from 10.53% to 8.58%) was observed, while for the standard one, the drop was about 25% (from 10.59% to 7.94%). This suggests that the infiltration of the perovskite in this NC-TiO_2 porous film is advantageous compared to the mesoporous TiO_2 layers with respect to the perovskite stability.

Conclusions

A simple, efficient, facile and industrially scalable method is presented here for the deposition of 1-dimensional nanocolumnar TiO_2 to be used as photoanodes in perovskite solar cells. Porous and homogeneous 1D-TiO_2 nanocolumnar thin films were fabricated through this proven methodology. The prepared photoanodes were then employed for perovskites solar cells fabrication and power conversion efficiencies close to 11% were obtained, which is the highest for TiO_2 1-dimensional nanostructures ever reported. This performance proves that the presented methodology can meet the standards required for practical application and large area integration. The thickness of TiO_2 and angle of deposition has bearing on its PV properties. NC-TiO_2 1-dimensional films thinner than the previous state of the art films utilized for perovskite solar cells were successfully implemented and yield an enhancement of the J_{SC} that has been related with an the increment of the porosity and the excellent infiltration of the absorber along the thin film structure. Nanocolumunar structures with 200nm thickness gave optimum efficiencies showing remarkable J_{SC} keeping V_{OC} and fill factor high. The facile electron collection in these 1-dimensional nanocolumns devices resulted in more stable systems than those mesoporous ones prepared by spin coating TiO_2. Surface analysis (SIMS, SEM) has shown that the perovskites are fully infiltrated in these nanocolumnar structures and fully cover the TiO_2 surface. We believe that the presented thin film process techniques brings new dimension for perovskite solar cells fabrication and for their industrial integration.

Acknowledgements

The ICMSE acknowledges the support Ministery of Economy and Competitiveness (projects MAT2013-40852-R and MAT2013-42900-P) and Torres Quevedo (SA) for the realization of this work. We also acknowledge support from "Quantcells" (CDTI), Spain.

References

1 H.-S. Kim, C.-R. Lee, J.-H. Im, K.-B. Lee, T. Moehl, A. Marchioro, S.-J. Moon, R. Humphry-Baker, J.-H. Yum, J. E. Moser, M. Grätzel, and N.-G. Park, *Sci. Rep.*, 2012, **2**, 591.
2 M. M. Lee, J. Teuscher, T. Miyasaka, T. N. Murakami, and H. J. Snaith, *Science (80)*, 2012, **338**, 643–647.
3 J. Burschka, N. Pellet, S.-J. Moon, R. Humphry-Baker, P. Gao, M. K. Nazeeruddin, and M. Grätzel, *Nature*, 2013, **499**, 316–9.
4 S. Kazim, M. K. Nazeeruddin, M. Grätzel, and S. Ahmad, *Angew. Chem. Int. Ed. Engl.*, 2014, **53**, 2812–24; *Angewandte Chemie*, 2014, **126**, 2854-2867.
5 N. J. Jeon, J. H. Noh, Y. C. Kim, W. S. Yang, S. Ryu, and S. Il Seok, *Nat. Mater.*, 2014, **13**, 897–903.
6 J.-H. Im, I.-H. Jang, N. Pellet, M. Grätzel, and N.-G. Park, *Nat. Nanotechnol.*, 2014, **9**, 927–932.
7 M. Liu, M. B. Johnston, and H. J. Snaith, *Nature*, 2013, **501**, 395–8.
8 Q. Chen, H. Zhou, Z. Hong, S. Luo, H.-S. Duan, H.-H. Wang, Y. Liu, G. Li, and Y. Yang, *J. Am. Chem. Soc.*, 2014, **136**, 622–5.
9 A. Mei, X. Li, L. Liu, Z. Ku, T. Liu, Y. Rong, M. Xu, M. Hu, J. Chen, Y. Yang, M. Gratzel, and H. Han, *Science (80-.).*, 2014, **345**, 295–298.
10 M. H. Kumar, N. Yantara, S. Dharani, M. Graetzel, S. Mhaisalkar, P. P. Boix, and N. Mathews, *Chem. commun.*, 2013, **49**, 11089–91.
11 F. J. Ramos, M. C. López-Santos, E. Guillén, M. K. Nazeeruddin, M. Grätzel, A. R. González-Elipe, and S. Ahmad, *ChemPhysChem*, 2014, **15**, 1148–1153.
12 J. T.-W. Wang, J. M. Ball, E. M. Barea, A. Abate, J. a Alexander-Webber, J. Huang, M. Saliba, I. Mora-Sero, J. Bisquert, H. J. Snaith, and R. J. Nicolas, *Nano Lett.*, 2013, **6**, 1739–1743.
13 D. Bi, L. Häggman, G. Boschloo, L. Yang, and E. M. J. Johansson, *RSC Adv.*, 2013, **3**, 18762–18766.
14 J. H. Heo, S. H. Im, J. H. Noh, T. N. Mandal, C.-S. Lim, J. A. Chang, Y. H. Lee, H. Kim, A. Sarkar, M. K. Nazeeruddin, M. Graetzel, and S. Il Seok, *Nat. Photon.*, 2013, **7**, 486–491.
15 P. Qin, S. Paek, M. I. Dar, N. Pellet, J. Ko, M. Grätzel, and M. K. Nazeeruddin, *J. Am. Chem. Soc.*, 2014, **136**, 8516–9.
16 H. Li, K. Fu, A. Hagfeldt, M. Grätzel, S. G. Mhaisalkar, and A. C. Grimsdale, *Angew. Chem. Int. Ed. Engl.*, 2014, **53**, 4085–8.
17 S. Ito, S. Tanaka, H. Vahlman, H. Nishino, K. Manabe, and P. Lund, *ChemPhysChem*, 2014, **15**, 1194–200.
18 J. M. Frost, K. T. Butler, F. Brivio, C. H. Hendon, M. van Schilfgaarde, and A. Walsh, *Nano Lett.*, 2014, **14**, 2584–2590.
19 V. W. Bergmann, S. A. L. Weber, F. J. Ramos, M. K. Nazeeruddin, M. Grätzel, D. Li, A. L. Domanski, I. Lieberwirth, S. Ahmad, and R. Berger, *Nat. Commun.*, 2014, **5:5001**, 1–9.
20 E. Guillén, F. J. Ramos, J. A. Anta, and S. Ahmad, *J. Phys. Chem. C*, 2014, **118 (40)**, 22913–22922.
21 B. Tian, X. Zheng, T. J. Kempa, Y. Fang, N. Yu, G. Yu, J. Huang, and C. M. Lieber, *Nature*, 2007, **449**, 885–889.

22 P. Krogstrup, H. I. Jørgensen, M. Heiss, O. Demichel, J. V. Holm, M. Aagesen, J. Nygard, and A. Fontcuberta i Morral, *Nat. Photon.*, 2013, **7**, 306–310.
23 Y. Liu, F. Zhang, and J. Wang, *Int. J. Photoenergy*, 2013, **Art. ID 34**, 1–6.
24 X. Feng, K. Shankar, O. K. Varghese, M. Paulose, T. J. Latempa, and C. A. Grimes, *Nano Lett.*, 2008, **8**, 3781–3786.
25 W.-Q. Wu, B.-X. Lei, H.-S. Rao, Y.-F. Xu, Y.-F. Wang, C.-Y. Su, and D.-B. Kuang, *Sci. Rep.*, 2013, **3:1352**, 1–7.
26 G. S. Han, S. Lee, J. H. Noh, H. S. Chung, J. H. Park, B. S. Swain, J.-H. Im, N.-G. Park, and H. S. Jung, *Nanoscale*, 2014, **6**, 6127–6132.
27 L. González-García, I. González-Valls, M. Lira-Cantu, A. Barranco, and A. R. González-Elipe, *Energy Environ. Sci.*, 2011, **4**, 3426–3435.
28 L. González-García, J. Parra-Barranco, J. R. Sánchez-Valencia, A. Barranco, A. Borrás, A. R. González-Elipe, M.-C. García-Gutiérrez, J. J. Hernández, D. R. Rueda, and T. a Ezquerra, *Nanotechnology*, 2012, **23**, 205701.
29 L. González-García, J. Idígoras, A. R. González-Elipe, A. Barranco, and J. A. Anta, *J. Photochem. Photobiol. A*, 2012, **241**, 58–66.
30 J. Qiu, Y. Qiu, K. Yan, M. Zhong, C. Mu, H. Yan, and S. Yang, *Nanoscale*, 2013, **5**, 3245–3248.
31 H.-S. Kim, J.-W. Lee, N. Yantara, P. P. Boix, S. A. Kulkarni, S. Mhaisalkar, M. Grätzel, and N.-G. Park, *Nano Lett.*, 2013, **13**, 2412–2417.
32 S. Dharani, H. K. Mulmudi, N. Yantara, P. T. Thu Trang, N.-G. Park, M. Graetzel, S. Mhaisalkar, N. Mathews, and P. P. Boix, *Nanoscale*, 2014, **6**, 1675–1679.
33 J.-H. Im, C.-R. Lee, J.-W. Lee, S.-W. Park, and N.-G. Park, *Nanoscale*, 2011, **3**, 4088.
34 Q. Jiang, X. Sheng, Y. Li, X. Feng, and T. Xu, *Chem. Commun.*, 2014, **50**, 14720–14723.
35 J.-W. Lee, S. H. Lee, H.-S. Ko, J. Kwon, J. H. Park, S. M. Kang, N. Ahn, M. Choi, J. K. Kim, and N.-G. Park, *J. Mater. Chem. A*, 2015, 3, 9179.

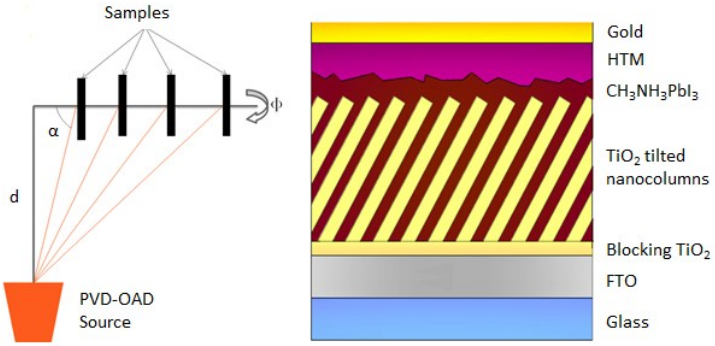

1-dimensional homogenous nanocolumunar structures prepared without any template method, for efficient perovskite solar cells fabrication.